THE JOURNAL OF PHYSICAL CHEMISTRY C

ARTICLE

pubs.acs.org/JPCC

Growth of Various TiO_2 Nanostructures for Dye-Sensitized Solar Cells

Fang Shao, Jing Sun,* Lian Gao,* Songwang Yang, and Jianqiang Luo

The State Key Lab of High Performance Ceramics and Superfine Microstructure, Shanghai Institute of Ceramics, Chinese Academy of Sciences, 1295 Ding Xi Road, Shanghai 200050, China

Supporting Information

ABSTRACT: Several kinds of one-dimensional TiO_2 nanostructures including nanorod arrays, nanobelt arrays, and fan-shaped rectangular parallelepiped rods were prepared by alkali hydrothermal method. Their morphology and crystalline phase could be controlled by changing the concentration of alkali solution. They were used as photoanodes to assemble front-side illumination dye-sensitized solar cells, and the cell performance was correlated with the nanostructure. The highest conversion efficiency (6.0%) was achieved with highly ordered TiO_2 nanorod arrays. We demonstrate that the oriented nanorods with appropriate lengths are beneficial to improve the electron transport property and thus lead to the increase of photocurrent, together enhancing the power conversion efficiency.

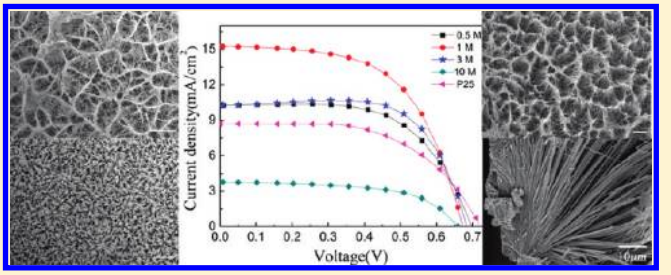

1. INTRODUCTION

In recent years, renewable sources have attracted more and more attention with the decrease of fossil fuel and the worsening of environmental pollution. Among these, dye-sensitized solar cells (DSSCs) created by Grätzel in 1991 have been a recognized and simple process.[1−5]

Central to the DSSC is a photoanode typically consisting of a monolayer of sensitizer (dye) adsorbed onto mesoporous TiO_2.[6] The traditional photoanodes composed of TiO_2 particles are believed to restrict the cell's performance due to the electron loss during percolation in the nanoparticle network.[7−9] On the contrary, one-dimensional (1D) nanostructure can provide direct conductive paths and reduce the electron recombination.[10−12] In particular, highly oriented TiO_2 nanoarrays are favored compared with random nanostructures.[8,13,14] Furthermore, as a photoanode, the geometry parameters of 1D TiO_2 nanostructures also play an important role in influencing the electron conduction.[4,15,16] Therefore, the fabrication of oriented 1D TiO_2 nanoarrays with controllable geometry is of great significance.

Various methods have been used to synthesize 1D TiO_2 nanostructures, such as electrochemical anodization,[17−21] sol−gel,[14,22,23] and hydrothermal methods.[11,24,25] Highly ordered TiO_2 nanotubes have been successfully fabricated by anodizing titanium foils and used as photoanodes for DSSCs. However, such photoanodes are opaque and thus back-side illumination geometry has to be used. This configuration is not desired for the following reasons:[26−29] (i) the high energy loss due to the low transmittance of the Pt sputtered transparent TCO glass; (ii) the high absorbance of the electrolyte; (iii) the increased travel distance for electrons to reach the collecting electrode. Instead, the front-side illumination DSSCs can overcome all shortcomings mentioned above.

In this paper, we successfully synthesized 1D TiO_2 nanostructures with different morphologies and constructed front-side illumination DSSCs based on them. The influence of geometry parameters was investigated in detail to cast light into better design for high efficiency DSSCs.

2. EXPERIMENTAL DETAILS

Fabrication of TiO_2 Nanostructures. TiO_2 structures were prepared on titanium foil by a three-step synthesis method. In the first step, the titanium plates (99.97% purity, 0.25 mm thickness, Sigma-Aldrich) were sonicated in distilled water, ethanol, and acetone to remove any impurities. Then they were put into 25 mL of 1 M NaOH aqueous in 50 mL Teflon-lined stainless steel autoclaves. The autoclaves were kept in an electric oven at 220 °C for 24 h. After cooling down to room temperature, samples were washed with deionized water and ethanol several times and dried at 60 °C for 10 min. In the second step, the samples were immersed in 0.6 M HCl for 2 h in order to exchange the Na^+ with H^+. In the last step, the as-prepared samples were calcined at 500 °C for 30 min. Moreover, effects of the NaOH concentration were also studied by varying the NaOH solution from 0.5 to 10 M.

Material Characterization. Crystallographic information of the obtained samples was observed using a powder X-ray diffraction (XRD, D/max 2550 V, Rigaku Tokyo, Japan). The morphology, size, and structure were examined with field emission scanning electron microscopy (FESEM, JSM-6700F, JEOL Tokyo, Japan) and transmission electron microscopy (TEM/HRTEM, JEM-200CX, JEOL

Received: November 10, 2010
Revised: December 3, 2010
Published: December 16, 2010

ACS Publications © 2010 American Chemical Society

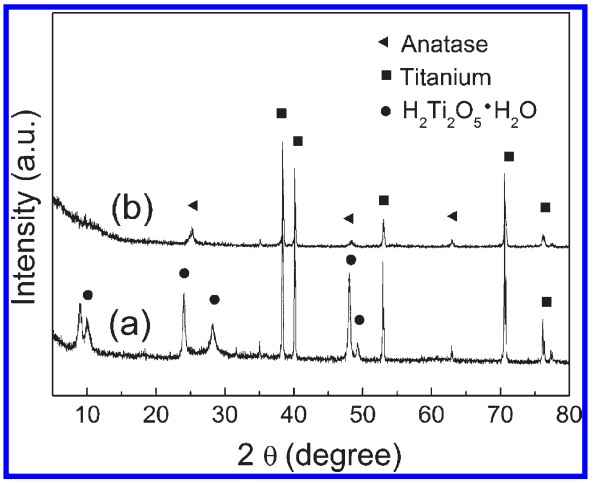

Figure 1. XRD of the nanostructured titanium foil surface after (a) ion exchange step and (b) annealing step when the NaOH concentration is 1 M.

Tokyo, Japan). The composition and contents of samples were investigated by energy dispersive spectrometer (EDS).

Solar Cell Fabrication. There were five different photoanodes prepared in this work. The DSSCs based on TiO_2 nanostructures grown in NaOH solution with different concentrations (0.5, 1, 3, and 10 M) are labeled as 0.5M-DSSC, 1M-DSSC, 3M-DSSC, and 10M-DSSC, respectively. To fabricate DSSCs, the substrates (FTO coated glasses) were first prepared by depositing a thin layer of nanocrystalline TiO_2 paste onto FTOs using a screen-printing method. The as-prepared TiO_2 membranes were then detached from the Ti plates and adhered onto the substrates as working electrodes. Besides, the DSSC comprised of commercial Degussa P25 TiO_2 nanoparticles (labeled as P25-DSSC) was formed using doctor-blading method as a comparison. All of the TiO_2 samples were dried under ambient conditions and annealed at 500 °C for 30 min. After cooling, they were chemically treated in a 0.2 M $TiCl_4$ solution at 60 °C for 1 h and then annealed at 450 °C for 30 min to improve the photocurrent and photovoltaic performances. When the temperature decreased to 80 °C, the obtained samples were soaked in 0.3 mM dye solution (solvent mixture of acetonitrile and *tert*-butyl alcohol in volume ratio of 1:1) and kept for 24 h at room temperature. Here the *cis*-bis(isothiocyanato)bis(2,2′-bipyridyl-4,4′-dicarboxylato)ruthenium(II) bis-(tetrabutyl ammonium) (N719) was used as the sensitizer. These dye-coated electrodes were assembled into solar cells with Pt-sputtered FTO counter electrodes and the electrolyte containing 0.5 M LiI, 0.05 M I_2, and 0.5 M *tert*-butylpyridine in acetonitrile.

Photovoltaic Characterization. Photoinduced photocurrent density−voltage ($J-V$) curves of the constructed solar cells were measured on an electrochemical workstation (model CHI 660C, CH) under an AM 1.5 illumination (100 mW/cm^2, model YSS-80A, Yamashita). Electrochemical impedance spectroscopic (EIS) curves of the DSSCs were also observed. The frequency range was from 0.1 Hz to 100 kHz. The applied bias voltage was set to the open-circuit voltage (V_{OC}) of the DSSC, which had been determined earlier. The incident photo to current conversion efficiency (IPCE) was detected by the spectral response measuring equipment (CEP-1500, Bunkoh-Keiki. Japan).

3. RESULTS AND DISCUSSION

Structural Characterization. XRD patterns of the obtained samples are shown in Figure 1. Curve a can be assigned to hydrated

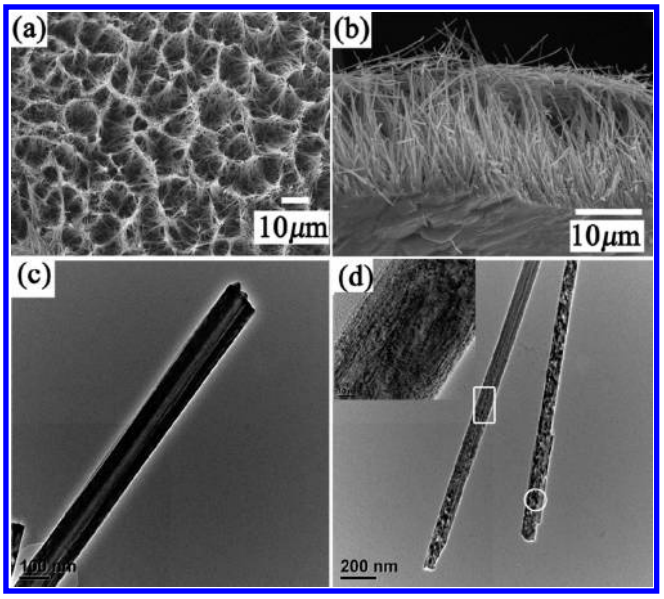

Figure 2. Morphological and structural characterization of $H_2Ti_2O_5 \cdot H_2O$ nanorods grown in 1 M NaOH for 24 h. (a, b) top view and cross-sectional view SEM images. (c) TEM image of a single nanotube. (d) nanotube−nanorod structures (left) and a multilayered nanorod (right). The inset image shows the HRTEM image taken from the area marked with the white circle.

dititanate ($H_2Ti_2O_5 \cdot H_2O$, JCPDS card No. 47-0124) while curve b was indexed to anatase TiO_2 (JCPDS card No.21-1272). The results show that $H_2Ti_2O_5 \cdot H_2O$ nanostructures were synthesized after hydrothermal and ion-exchange processes and completely converted to anatase TiO_2 by calcinating at 500 °C for 30 min.

As shown by the SEM images in Figure 2a,b, the $H_2Ti_2O_5 \cdot H_2O$ exhibits a nanowire morphology which is nearly perpendicular to the substrate. TEM images indicate that the nanoarrays include nanotubes and multilayered nanorods (Figure 2c,d). The average diameter of nanotubes is about 65 nm with an approximate inner diameter of 17 nm. Nanorods have almost exactly the same size as nanotubes. There are many slit pores in nanorods, and the edge dislocations are apparent. Meanwhile, nanowires composed of both nanotube and multilayered nanorod structures are also observed, such as the left one marked with a white rectangle in Figure 2d. EDS results indicate that the Ti and O concentrations of the nanotubes and nanorods are 28.11 and 71.89 atom %, respectively, roughly corresponding to the atomic ratio of $H_2Ti_2O_5 \cdot H_2O$ (Figure S1, Supporting Information). When the reaction time increased to 48 h, there were nearly no nanotubes existing (Figure S2, Supporting Information). On the basis of the above results, it can be deduced that nanotubes gradually split into multilayered nanorods.

Figure 3 shows SEM and TEM images of the TiO_2 nanowires being calcinated at 500 °C for 30 min. From the cross-sectional and top-view images of the TiO_2 (Figure 3a,b), it clearly shows that the highly ordered nanoarray morphology was preserved. The diameter remains almost unchanged while the pore shrinkage was pronounced. The HRTEM image (Figure 3d) shows a lattice spacing of 0.352 nm, which corresponds to the (101) plane of anatase. EDS curve of the calcined product (Figure S3, Supporting Information) reveals the presence of Ti and O as the only elementary components and the atomic ratio of Ti and O was about 1:2.

The Influence of Alkaline Concentration. To investtigate the NaOH concentration influence, we have carried out hydrothermal

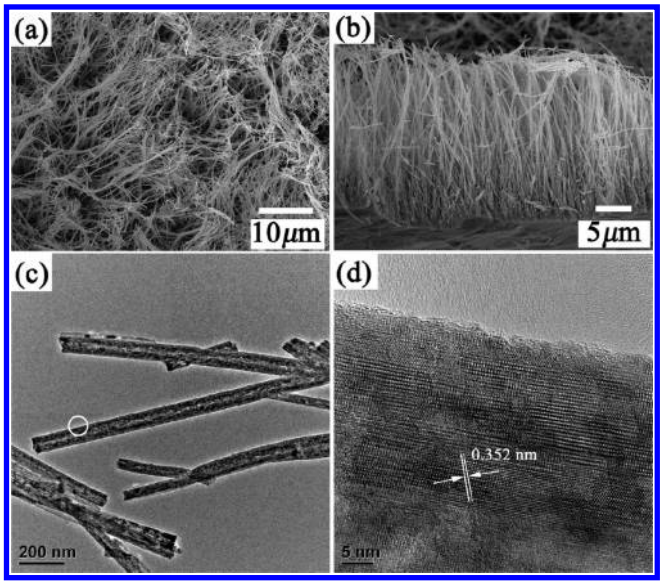

Figure 3. (a, b) Top-view and cross-sectional view SEM images of the TiO_2 obtained by calcining at 500 °C for 30 min. (c) TEM image of the obtained TiO_2 nanowires. (d) HRTEM image taken from the area marked with the white circle in (c).

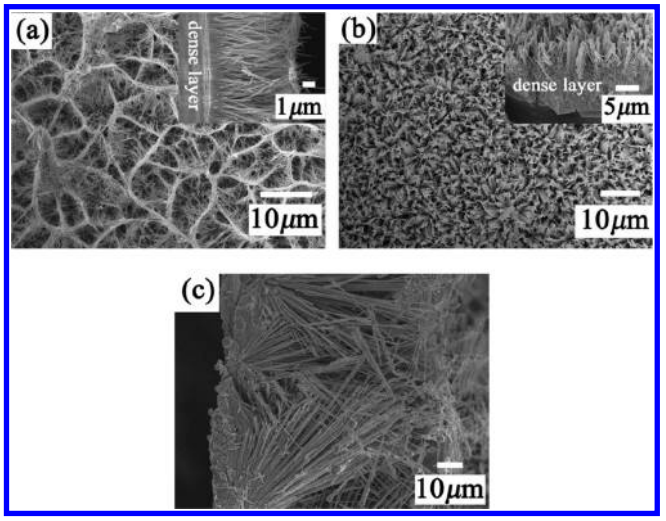

Figure 4. SEM images of the as-prepared nanostructures grown in NaOH aqueous with different concentrations: (a) 0.5 M, (b) 3 M, (c) 10 M. The inset images in (a) and (b) show the corresponding morphology at higher resolution.

experiments with solutions containing 0.5, 3, and 10 M NaOH. Morphologies of the obtained products are given in Figure 4. With 0.5 M NaOH, the as-prepared $H_2Ti_2O_5 \cdot H_2O$ presented a morphology of nanowire array with length of ~5.6 μm (Figure 4a). When the NaOH concentration came up to 3 M, a nanobelt array was obtained, and the length of arrays increased to ~8.5 μm (Figure 4b). It should be noticed that a dense thick transitional layer was formed at the bottom of the nanoarray structures for 0.5 and 3 M concentrations. On the contrary, the dense layer was fairly thin in the 1 M case (Figure 2b). The formation process of the nanorods and naobelts which were perpendicular to the substrate can be proposed as follows. In the beginning, the Ti plate reacted with NaOH and formed $Na_2Ti_2O_5 \cdot H_2O$ nanocrystallines on the surface. Then, nanorods or nanobelts began to grow from $Na_2Ti_2O_5 \cdot H_2O$ nanocrystallines

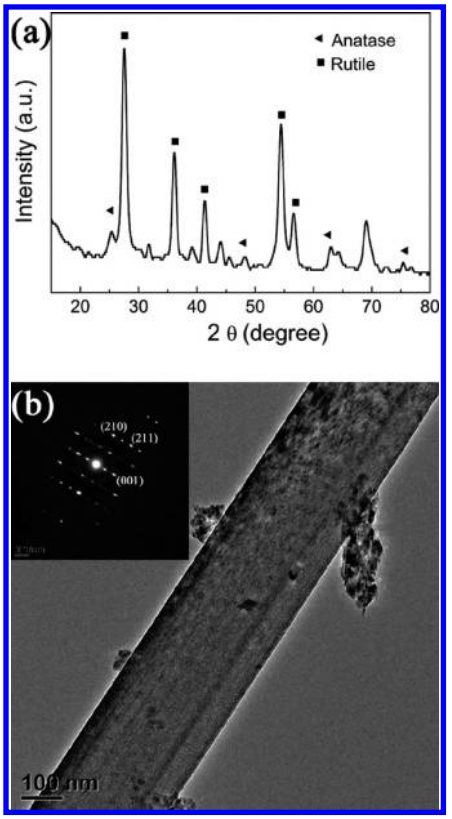

Figure 5. (a) XRD pattern of the film formed in 10 M NaOH after calcination. (b) The TEM image of an individual rectangular parallelepiped rod. Inset image is the corresponding SAED pattern.

which acted as nuclei in the hydrothermal process. Meanwhile, the Ti atoms inside diffused to the surface to supply Ti source. The nanostructures were grown nearly perpendicular to the substrate, since there were too many nuclei to grow in the cross direction. This process can be explained by "nucleation−dissolution−recrystallization" growth mechanism.

When the NaOH concentration is increased to 10 M, the fan-shaped structure with thickness of ~75 μm appeared (Figure 4c). A closer look at the film in cross section (Figure S4a, Supporting Information) shows that nanorods initially radiate from the nucleation site and the inclined nanorods obstruct each other. However, the nanorods show alignment in the vertical direction to a certain extent. The reason could be that only the nanorods perpendicular to the substrate can grow freely. Moreover, from the high-resolution SEM image in Figure S4b (Supporting Information), it is clear that the nanorods in fact are rectangular parallelepiped rods. The width and height are ~300 and ~180 nm, respectively.

It is worth noting that the NaOH concentration changes not only the morphology but also the crystalline phase of the obtained TiO_2. The XRD pattern of the TiO_2 obtained with 10 M NaOH exhibits the characteristic peaks of both anatase and rutile phases (Figure 5a). Figure 5b shows the TEM image of an individual cuboid and the corresponding SAED pattern, which reveals that the rectangular parallelepiped rods grow along the [001] direction.

Solar Cell Properties. Figure 6 shows the current density−voltage curves of the open cells based on different TiO_2 photoelectrodes. The resultant photovoltaic parameters are summarized in Table 1. Compared with P25-DSSC, 1M-DSSC presented

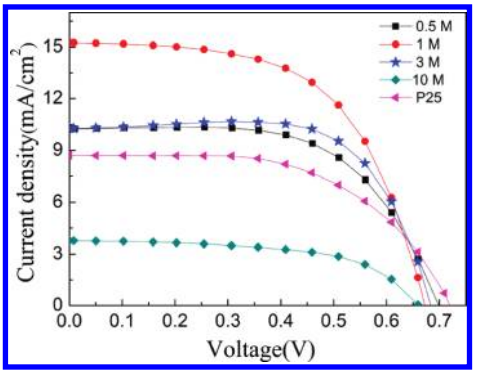

Figure 6. *J-V* characteristics of dye-sensitized solar cells assembled with TiO_2 films prepared with different concentrations of aqueous NaOH and P25.

Table 1. Performance Characteristics of DSSCs Based on Photoanodes of Various TiO_2 Nanostructures and P25

DSSCs	V_{OC} (V)	J_{SC} (mA cm^{-2})	FF (%)	η (%)	thickness (μm)
0.5M-DSSC	0.70	10.26	61.21	4.40	11.68
1M-DSSC	0.67	15.25	58.33	6.00	15.11
3M-DSSC	0.69	10.29	68.87	4.86	24.10
10M-DSSC	0.66	3.71	58.68	1.44	*a*
P25-DSSC	0.72	8.90	56.03	3.60	14.99

[a] Too thick to be measured.

significantly increased short-circuit photocurrent density (J_{sc}) by 71.3% from 8.90 to 15.25 mA/cm^2, and the overall power conversion efficiency ($\eta = J_{SC}V_{OC}FF/P_{in}$ with P_{in} = 100 mW cm^2) was enhanced by 66.7% from 3.6% to 6.0%. The average thickness of P25 film was experimentally controlled to be identical to that of 1 M film (~15 μm). The performances of 0.5M-DSSC and 3M-DSSC were also better than P25-DSSC. This may be due to the directed electron pathway along the long axis of the 1D nanostructure.[10] Besides, nanorods and nanobelts have fewer interparticle connections, which decrease the recombination sites.[7]

Over the range of NaOH concentrations, η increased from 4.40% at 0.5 M to a maximum value of 6.0% at 1 M and then declined to 4.86% at 3 M. The 10 M cell displayed the lowest photovoltaic performance of 1.4%. Increase of nanorod length increases the surface area, which favors more dye loading. This may be one of the possible reasons for the increased J_{sc} from 0.5M-DSSC to 1M-DSSC. However, too thick a film is undesirable. The reduction of the J_{sc} of 3 M-DSSC may be partly due to the fact that the electron diffusion length (L_n) is shorter than the thickness at a value of 24.10 μm. The electron diffusion length is the average distance that an injected electron can travel through the photoelectrode before recombination.[4,30] It has been reported that the L_n value of the photoelectrode based on TiO_2 nanorods was 11.4 μm.[8] Therefore, significant portions of the injected charges in 3M-DSSC will be lost before collected. Besides, the thick dense layer of the TiO_2 in 0.5 and 3 M DSSCs may also influence the J_{sc}. The 10M-DSSC displayed a relatively poor photovoltaic performance. The reasons are as follows:[31−35] the increase in charge recombination on account of the too thick TiO_2 film; the lower specific surface area due to the distinct structure; the slow mobility probably due to the original rutile property of larger electron effective mass.

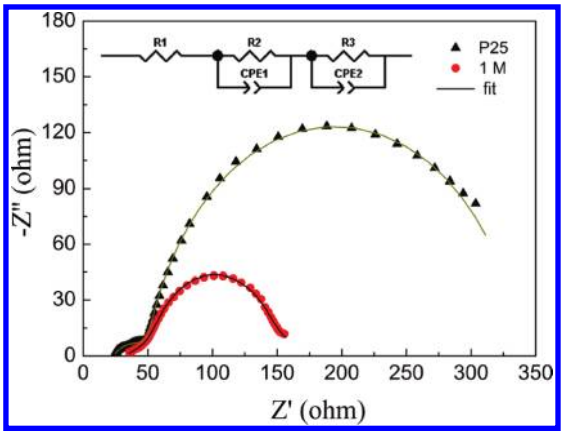

Figure 7. Electrochemical impedance spectra of 1 M DSSC and P25-DSSC.

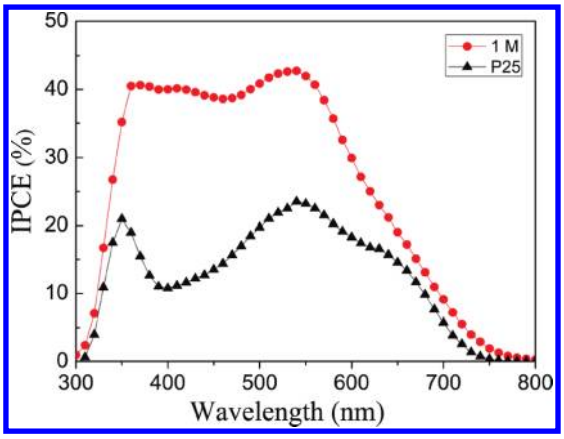

Figure 8. IPCE curves of 1M DSSC and P25-DSSC.

In order to investigate the electron transport property in TiO_2 film electrodes, electrochemical impedance spectroscopy (EIS) measurements were employed in the frequency range of 0.1 Hz to 100 kHz. Figure 7 shows the Nyquist plots of 1M-DSSC and P25-DSSC measured at forward bias of the open-circuit voltage under 100 mW cm^{-2}. According to the EIS model reported in the literature,[36−38] the smaller semicircle occurring at higher frequencies is related to the parallel connection of charge-transfer resistance (R_{Pt}) and the interfacial capacitance (C_{Pt}) at the counter electrode/electrolyte interface. The larger one at the lower frequency region is attributed to the combination of charge-transfer resistance occurring at the TiO_2/dye/electrolyte interface (R_{ct}) and the chemical capacitance that stands for the change of electron density as a function of the Fermi level (C_μ). Finally, the small feature at the lowest frequencies which is not observable here is the effect of the diffusion of the ions in the electrolyte.

Compared with P25-DSSC, the semicircle size in the middle-frequency region of 1M-DSSC reduced, owing to the acceleration of electron transfer process in the photoanode.[39] Furthermore, the charge transfer resistance of the DSSCs was analyzed by Z-view software using an equivalent circuit containing constant phase elements (CPE) and resistances (R) (Figure 7, inset). In the absence of a change in the other elements of impedance, we are concerned here only with the larger semicircles. The fitting values of R_{ct} corresponding to 1M-DSSC and P25-DSSC are 73.46 and 285.9 Ω, respectively. The low transfer resistance

could be an important factor for the improvement of the photoelectrochemical performance of the TiO_2 nanorod arrays.

The IPCE is defined as the number of electrons in the external circuit under short circuit conditions per incident photon at a given wavelength.[36,40] IPCE spectra as a function of wavelength for 1M-DSSC and P25-DSSC are shown in Figure 8. Compared with P25-DSSC, the quantum efficiencies were enhanced over the whole spectral range and exhibited a maximum of 43% at 540 nm for 1M-DSSC.

4. CONCLUSION

In this work, TiO_2 nanostructures with various morphologies were obtained by an alkali hydrothermal treatment and annealing, and they were successfully applied as photoanode materials in front-side illumination DSSCs. The change of NaOH concentrations strongly alters the morphology and crystal phase of the nanostructures, which, in turn, significantly affects the electron transport and the solar energy conversion properties of DSSCs. Rutile appeared in the fan-shaped TiO_2 rectangular parallelepiped rods when the NaOH concentration increased to 10 M and the lowest η was observed. An overall 6.0% energy-conversion efficiency was obtained for the 1M-DSSC, which has an improvement of 66.7% relative to that of P25-DSSC. The improvement was ascribed to the enhanced electron injection and transfer efficiency, which was verified by EIS analysis. A systematic investigation on the effect of NaOH concentration will provide valuable insight for the controlled synthesis of TiO_2 nanostructures and the design of high-performance DSSCs.

■ ASSOCIATED CONTENT

Supporting Information. EDS patterns of $H_2Ti_2O_5 \cdot H_2O$ and TiO_2, TEM images of $H_2Ti_2O_5 \cdot H_2O$ nanostructures grown in 1 M NaOH for 48 h, and SEM images of the rectangular parallelepiped rods prepared with 10 M NaOH solution. This material is available free of charge via the Internet at http://pubs.acs.org.

■ AUTHOR INFORMATION

Corresponding Author

*E-mail addresses: jingsun@mail.sic.ac.cn (J. Sun) and liangao@mail.sic.ac.cn (L. Gao).

■ ACKNOWLEDGMENT

This work was supported by the National Natural Science Foundation of China (Grant No. 50972157, 51072215).

■ REFERENCES

(1) Oregan, B.; Gratzel, M. *Nature* **1991,** *353*, 737.
(2) Sauvage, F.; Chen, D. H.; Comte, P.; Huang, F. Z.; Heiniger, L. P.; Cheng, Y. B.; Caruso, R. A.; Graetzel, M. *ACS Nano* **2010,** *4*, 4420.
(3) Wang, Q.; Ito, S.; Gratzel, M.; Fabregat-Santiago, F.; Mora-Sero, I.; Bisquert, J.; Bessho, T.; Imai, H. *J. Phys. Chem. B* **2006,** *110*, 25210.
(4) Lee, B. H.; Song, M. Y.; Jang, S. Y.; Jo, S. M.; Kwak, S. Y.; Kim, D. Y. *J. Phys. Chem. C* **2009,** *113*, 21453.
(5) Longo, C.; Nogueira, A. F.; De Paoli, M. A.; Cachet, H. *J. Phys. Chem. B* **2002,** *106*, 5925.
(6) Lopez-Luke, T.; Wolcott, A.; Xu, L. P.; Chen, S. W.; Wcn, Z. H.; Li, J. H.; De La Rosa, E.; Zhang, J. Z. *J. Phys. Chem. C* **2008,** *112*, 1282.
(7) Law, M.; Greene, L. E.; Johnson, J. C.; Saykally, R.; Yang, P. D. *Nat. Mater.* **2005,** *4*, 455.
(8) Zhu, K.; Neale, N. R.; Miedaner, A.; Frank, A. J. *Nano Lett.* **2007,** *7*, 69.
(9) Chen, D.; Zhang, H.; Hu, S.; Li, J. H. *J. Phys. Chem. C* **2008,** *112*, 117.
(10) Kang, S. H.; Choi, S. H.; Kang, M. S.; Kim, J. Y.; Kim, H. S.; Hyeon, T.; Sung, Y. E. *Adv. Mater.* **2008,** *20*, 54.
(11) Yang, W. G.; Wan, F. R.; Wang, Y. L.; Jiang, C. H. *Appl. Phys. Lett.* **2009,** *95*, 133121.
(12) Fujihara, K.; Kumar, A.; Jose, R.; Ramakrishna, S.; Uchida, S. *Nanotechnology* **2007,** *18*, 365709.
(13) Wang, H. E.; Chen, Z. H.; Leung, Y. H.; Luan, C. Y.; Liu, C. P.; Tang, Y. B.; Yan, C.; Zhang, W. J.; Zapien, J. A.; Bello, I.; Lee, S. T. *Appl. Phys. Lett.* **2010,** *96*, 263104.
(14) Kang, T. S.; Smith, A. P.; Taylor, B. E.; Durstock, M. F. *Nano Lett.* **2009,** *9*, 601.
(15) Oh, J. K.; Lee, J. K.; Kim, H. S.; Han, S. B.; Park, K. W. *Chem. Mater.* **2010,** *22*, 1114.
(16) Lee, K. M.; Suryanarayanan, V.; Ho, K. C. *J. Power Sources* **2009,** *188*, 635.
(17) Li, L. L.; Tsai, C. Y.; Wu, H. P.; Chen, C. C.; Diau, E. W. G. *J. Mater. Chem.* **2010,** *20*, 2753.
(18) Kuang, D.; Brillet, J.; Chen, P.; Takata, M.; Uchida, S.; Miura, H.; Sumioka, K.; Zakeeruddin, S. M.; Gratzel, M. *ACS Nano* **2008,** *2*, 1113.
(19) Chun, K. Y.; Park, B. W.; Sung, Y. M.; Kwak, D. J.; Hyun, Y. T.; Park, M. W. *Thin Solid Films* **2009,** *517*, 4196.
(20) Shankar, K.; Mor, G. K.; Prakasam, H. E.; Yoriya, S.; Paulose, M.; Varghese, O. K.; Grimes, C. A. *Nanotechnology* **2007,** *18*, 065707.
(21) Yin, H.; Liu, H.; Shen, W. Z. *Nanotechnology* **2010,** *21*, 035601.
(22) Lei, Y.; Zhang, L. D.; Meng, G. W.; Li, G. H.; Zhang, X. Y.; Liang, C. H.; Chen, W.; Wang, S. X. *Appl. Phys. Lett.* **2001,** *78*, 1125.
(23) Attar, A. S.; Ghamsari, M. S.; Hajiesmaeilbaigi, F.; Mirdamadi, S.; Katagiri, K.; Koumoto, K. *Mater. Chem. Phys.* **2009,** *113*, 856.
(24) Morgan, D. L.; Liu, H. W.; Frost, R. L.; Waclawik, E. R. *J. Phys. Chem. C* **2010,** *114*, 101.
(25) Jiu, J. T.; Isoda, S.; Wang, F. M.; Adachi, M. *J. Phys. Chem. B* **2006,** *110*, 2087.
(26) Xu, C. K.; Shin, P. H.; Cao, L. L.; Wu, J. M.; Gao, D. *Chem. Mater.* **2010,** *22*, 143.
(27) Mor, G. K.; Shankar, K.; Paulose, M.; Varghese, O. K.; Grimes, C. A. *Nano Lett.* **2006,** *6*, 215.
(28) Park, J. H.; Lee, T. W.; Kang, M. G. *Chem. Commun.* **2008,** 2867.
(29) Chen, Q. W.; Xu, D. S. *J. Phys. Chem. C* **2009,** *113*, 6310.
(30) Peter, L. M.; Wijayantha, K. G. U. *Electrochem. Commun.* **1999,** *1*, 576.
(31) Park, N. G.; van de Lagemaat, J.; Frank, A. J. *J. Phys. Chem. B* **2000,** *104*, 8989.
(32) Xu, H.; Tao, X.; Wang, D. T.; Zheng, Y. Z.; Chen, J. F. *Electrochim. Acta* **2010,** *55*, 2280.
(33) van de Lagemaat, J.; Park, N. G.; Frank, A. J. *J. Phys. Chem. B* **2000,** *104*, 2044.
(34) Jung, H. S.; Kim, H. *Electron. Mater. Lett.* **2009,** *5*, 73.
(35) Kang, S. H.; Kang, M. S.; Kim, H. S.; Kim, J. Y.; Chung, Y. H.; Smyri, W. H.; Sung, Y. E. *J. Power Sources* **2008,** *184*, 331.
(36) Jose, R.; Thavasi, V.; Ramakrishna, S. *J. Am. Ceram. Soc.* **2009,** *92*, 289.
(37) Wang, Q.; Moser, J. E.; Gratzel, M. *J. Phys. Chem. B* **2005,** *109*, 14945.
(38) Chen, J. K.; Li, K. X.; Luo, Y. H.; Guo, X. Z.; Li, D. M.; Deng, M. H.; Huang, S. Q.; Meng, Q. B. *Carbon* **2009,** *47*, 2704.
(39) Sun, S. R.; Gao, L.; Liu, Y. Q. *Appl. Phys. Lett.* **2010,** *96*, 083113.
(40) Sauvage, F.; Di Fonzo, F.; Bassi, A. L.; Casari, C. S.; Russo, V.; Divitini, G.; Ducati, C.; Bottani, C. E.; Comte, P.; Graetzel, M. *Nano Lett.* **2010,** *10*, 2562.